Temperature-dependent synchrotron powder diffraction phase studies of $(K_{0.37}Na_{0.52}Li_{0.03})(Nb_{0.87}Ta_{0.1}Sb_{0.03})O_3$ ferroelectric ceramics

Henry E. Mgbemere[I], Rodrigo P. Fernandes[I], Manuel Hinterstein[II] and Gerold A. Schneider*[,I]

[I] Institute of Advanced Ceramics, Hamburg University of Technology, Denickestr. 15, 21073 Hamburg, Germany
[II] Institute of Materials Science, TU Dresden, Helmholtzstr. 7, 01062 Dresden, Germany

Received July 12, 2010; accepted October 5, 2010

Synchrotron XRD / Rietveld refinement / Lead-free ferroelectric ceramics / Potassium sodium niobate / High temperature

Abstract. Temperature-dependent synchrotron powder diffraction measurements have been performed on lead-free ferroelectric $(K_{0.37}Na_{0.52}Li_{0.03})(Nb_{0.87}Ta_{0.1}Sb_{0.03})O_3$ ceramics. The measurement was performed from 20 °C to 400 °C with 20 °C steps. The diffraction patterns showed the existence of two phases from 20 °C to 180 °C while the ferroelectric to paraelectric phase transition occurred between 340 °C and 360 °C. Rietveld refinement using the Fullprof software was employed and the two-phase region was refined using a combination of the orthorhombic phase with space group *Amm*2 (38) and the tetragonal phase with space group *P*4*mm* (99) from 20 °C to 180 °C. The tetragonal phase was used for the refinement up to 340 °C while the cubic phase was refined with space group $Pm\bar{3}m$ (221). Good refinement structure parameters were obtained for all temperatures with the average G.O.F being approximately 4.0. Information about the cell parameters and weight fraction of the phases were obtained as a function of temperature.

Introduction

Lead zirconate titanate (PZT) based piezoelectric ceramics are currently the most used in the manufacture of actuators, sensors and other electromechanical devices. Lead is a toxic element and therefore environmentally unfriendly, so there is a need to replace PZT with less toxic piezoelectric ceramics. There are many possible alternatives for their replacement among which the potassium sodium niobate $(K_xNa_{1-x})NbO_3$ (KNN) based ceramics are one of the most promising, having a high Curie temperature and moderate piezoelectric charge coefficients [1].

Pure KNN is difficult to synthesize and compared to PZT, its piezoelectric coefficients are low. It has been reported that when isovalent elements like Li, Ta and Sb (0.04, 0.1 and 0.04 moles respectively) are added to KNN, their piezoelectric properties are improved [2]. The authors attributed this improvement in piezoelectric properties to the occurrence of a morphotropic phase boundary (MPB). It has been suggested that at this phase boundary, a coupling between different polarization directions enhances the piezoelectric properties. A MPB is well known to exist in PZT [3]. For a piezoelectric ceramic to be classified as having a MPB, the piezoelectric properties should not depend heavily on temperature [4]. Some researchers have investigated the temperature dependence of the piezoelectric coefficients of Li-, Ta- and Sb-modified KNN and found a strong correlation between increasing piezoelectric coefficients and decreasing phase transition temperature [5]. They proposed the term "polymorphic phase transition" (PPT) as being more appropriate since both the Curie temperature (T_C) and the temperature at which the tetragonal to orthorhombic (T_{T-O}) transition takes place are shifted to lower values in comparison to pure KNN [5, 6]. The piezoelectric and electromechanical properties of Li-, Ta- and Sb-modified KNN ceramics are however high and have generated a lot of interest from researchers around the world. It is known that there are more than one phase in the above stated composition but the structure has not been well studied like in the case of pure KNN. According to Akdogan *et al.* [7], the room-temperature state of KNN ceramics doped with Li, Ta and Sb consists of two ferroelectric phases, tetragonal and orthorhombic. The authors assigned the structure of the tetragonal phase to *P*4*mm*, while that of the orthorhombic phase to *Pmm*2 with all reflections allowed. Akdogan *et al.* ruled out *Amm*2 as a possible orthorhombic phase arguing that it has an "unrealistically" large volume for a perovskite with a primitive unit cell. They claimed that such a large volume should correspond to a doubled unit cell, which in turn implies an anti-ferroelectric state and such a state was not revealed by hysteresis loop measurements [7]. Actually, in *Amm*2 two of the fundamental translation vectors are along the cubic {110} directions, instead of all three to be along {100} as in the case of *P*4*mm* and *Pmm*2. Hence, the unit-cell volume of *Amm*2 is considerably larger as compared to $Pm\bar{3}m$, without requiring a doubling of the unit cell and a consequent anti-ferroelectric state. A textbook example for a ferroelectric single-perovskite material with *Amm*2 symmetry is $BaTiO_3$. Therefore, *Amm*2

* Correspondence author (e-mail: g.schneider@tu-harburg.de)

is also a plausible symmetry for the orthorhombic phase of modified KNN ceramics. $(K_xNa_{1-x})NbO_3$ ceramics are a solid solution of ferroelectric $KNbO_3$ and anti-ferroelectric $NaNbO_3$. Studies on this material have been reported since the 1950's with some of the publications mainly focused on determining their piezoelectric and electro-mechanical properties. Structural studies were presented on $NaNbO_3$ and $KNbO_3$ [8, 9]. A detailed phase diagram of KNN ceramics was published by Ahtee and Glazer where the lattice parameters and tilted octahedral settings in this solid solution were presented [10]. At room temperature, there are phase boundaries at $x \approx 0.18$, 0.35 and 0.48 respectively.

Recently, more research has been carried out on the structural properties of this composition using different techniques. A combination of a theoretical and experimental approach to investigate the properties of KNN at $x = 0.5$ has been reported where it was stated that a rhombohedral phase exists at room temperature which could not be detected earlier using X-ray diffraction [11]. A detailed structural study of $(K_xNa_{1-x})NbO_3$ has also been carried out where x ranges from 0.24 to 0.36 and the results presented varied slightly from previous reports with a phase coexistence region at the transition between monoclinic and tetragonal phases [12]. Evidence was also found to support the earlier assertion that intermediate oxygen octahedral tilting is present in the tetragonal phase. Low temperature studies have been made at $x = 0.05$ and $x = 0.3$ which showed that the structures have a rhombohedral symmetry with a space group $R3c$ and a tilt system $a^-a^-a^-$ [13].

There are little or no studies on the structural properties of KNN modified with lithium, tantalum and antimony at elevated temperatures. In this investigation, KNN modified with Li, Ta and Sb was chosen because it has so far, one of the highest piezoelectric properties of lead-free piezoelectric ceramics [2]. The objective of this article therefore is to determine quantitatively the relative amount of the phases present, their lattice parameters as they change with temperature and their phase transition temperatures.

Experimental details

Sample preparation

The sample was produced through the conventional ceramic solid state reaction method. K_2CO_3, Na_2CO_3, Li_2CO_3 (99%), Nb_2O_5, Ta_2O_5 and Sb_2O_3 (99.9%) (Chempur Feinchemikalien und Forschungs GmbH, Karlsruhe, Germany) were used as the starting powders for the synthesis. The nominal composition originally intended to be synthesized was $(K_{0.43}Na_{0.53}Li_{0.04})(Nb_{0.86}Ta_{0.1}Sb_{0.04})O_3$. After drying the powders at 200 °C for 4 h, they were mixed and attrition milled for 4 h and then calcined in air at 750 °C for 4 h. The milling and calcination steps were repeated to homogenize the powder and also to ensure that the required phase was formed. The mixture was pressed into a disc of 12.5 mm diameter first using a uniaxial press at 170 MPa and later with a cold isostatic press at 500 MPa for 2 min. The pellets were sintered in air at 1075 °C for 1 h with a heating and cooling rate of 3 °C/min and 10 °C/min respectively. The pellets were ground for both chemical analysis and synchrotron X-ray diffraction measurement. In order to reduce residual stresses, the samples were annealed at 750 °C for 30 min.

Optical emission spectroscopy/Inductive coupled plasma (OES-ICP (PE-Optima 7000 DV)) characterization technique was used to determine quantitatively the amount of each element present and possible elements introduced during processing. Four separate measurements were made and the values were averaged to obtain the final result. The results of the OES-ICP analysis are shown in Table 1. Some of the elements with a lower melting temperature (Li, K and Sb) were lost due to sublimation during the sintering process with the highest loss being observed for Sb. As a result, the sample contains vacancies on the A-site of the perovskite structure.

Elements like Na, Nb, Ta and O had slightly higher amounts than calculated for the synthesis. Since the starting powders are not 100% pure, it is possible that some of the powders contained small amounts of these powders in excess. The final composition was adjusted to reflect the changes in the amounts of elements present after the chemical analysis. Zirconia balls were used to mill the powders and the analysis showed that 0.91 g/kg of zirconium was present in the sample. It was assigned to the A-site of the perovskite for the refinement. Finally, we concluded that our actual composition is $(K_{0.37}Na_{0.52}Li_{0.03})(Nb_{0.87}Ta_{0.1}Sb_{0.03})O_3$.

Synchrotron X-ray data collection and refinement

The synchrotron X-ray diffraction data were collected at the synchrotron facility (HASYLAB/DESY beamline B2) in Hamburg from 20 °C to 400 °C in steps of 20 °C. High temperature measurements were performed using a capillary furnace from Stoe & Cie type 0.65.3. Data were recorded by a position sensitive detector [14] at a wavelength of 0.6881Å. More details about the experimental setup at the beamline can be found in the Ref. [14, 15].

All the collected data were refined by the Rietveld method using Fullprof suite [16]. Due to phase coexistence (orthorhombic-tetragonal) in the collected diffraction

Table 1. OES-ICP analysis data as well as calculated molar amounts of the elements in our composition.

Element	Li	Na	K	Nb	Sb	Ta	O	Zr[a]
OES-ICP values [g/kg]	1.270(3)	67.90(14)	83.60(17)	463.0(9)	19.60(4)	109.0(2)	266.0(5)	0.91
Element amount [mol]	0.0317	0.515	0.372	0.867	0.028	0.105	3.0	0.0017

a: This element was introduced into the powder during processing.

patterns over a wide range of temperatures (20 °C to 180 °C), a two-phase model of orthorhombic *Amm*2 and tetragonal *P*4*mm* was used for the refinement. In *Amm2,* the different values of b_o and c_o lead to a rhombic distortion of the $(001)_C$ plane resulting in an expansion along $[110]_C$. The subscript 'o' denotes the orthorhombic cell. Due to symmetry restrictions, the amount of refinable parameters in *Amm2* is smaller than in *Pmm*2. Therefore *Amm*2 was used instead of *Pmm*2. Between 200 °C and 320 °C a single phase model with *P*4*mm* was applied. Above 340 °C, the *P*4*mm* phase was no longer appropriate, so the refinement did converge further up to 400 °C using the $Pm\bar{3}m$ space group. The background under the peaks was refined using a linear interpolation between points from the regions in which no reflections contributed to the intensity. The model used was based on a T–C–H pseudo-Voigt profile function which is convoluted with asymmetry due to axial divergence as formulated by [17] and using the method of Finger *et al.* [18, 19]. The atomic positions were refined for the oxygen and B-site cations while the isotropic atomic displacement parameters B_{iso} were refined for all the elements. Efforts to refine the structure using anisotropic displacement parameter were not successful. The broadening model in the general strain formulation was used to refine the strain in the sample [20]. The full experimental details and refinement results for some selected temperatures are as given in Table 3. The crystal structure image was produced using the crystallographic software DIAMOND [21].

Temperature dependent measurement of dielectric constant

The samples were coated on both surfaces with silver paints which acted as electrodes for the dielectric property measurement. The temperature dependence of the dielectric properties of the ceramics was measured from 20 Hz to 1 MHz with an LCR meter (HP 4284A, Agilent Technologies, Inc., Palo Alto, USA) connected to a heating chamber.

Results and discussion

Figure 1 shows the observed and calculated diffraction profiles and their difference curves for $(K_{0.37}Na_{0.52}Li_{0.03})(Nb_{0.87}Ta_{0.1}Sb_{0.03})O_3$ at 20 °C, 200 °C and 360 °C respectively. Figure 1a shows the profile at 20 °C where the two-phase model was used to refine the structure while Fig. 1b and c show the profiles where a single phase model (tetragonal and cubic, respectively) was used. The enlarged insets in Fig.s 1a to c indicate the higher 2-theta regions (35 ° to 50 °) in the diffraction patterns. The splitting of the peaks due to the two-phase composition can be seen in Fig. 1a, while in Fig. 1b the single phase tetragonal splitting can be observed. The inset in Fig. 1c depicts no reflection splitting for the cubic phase.

Table 2 gives the fractional atomic coordinates and isotropic displacement parameters for some refinements at selected temperatures showing the two phase regions (20 °C and 100 °C), single phase tetragonal region (200 °C) and the cubic phase (360 °C).

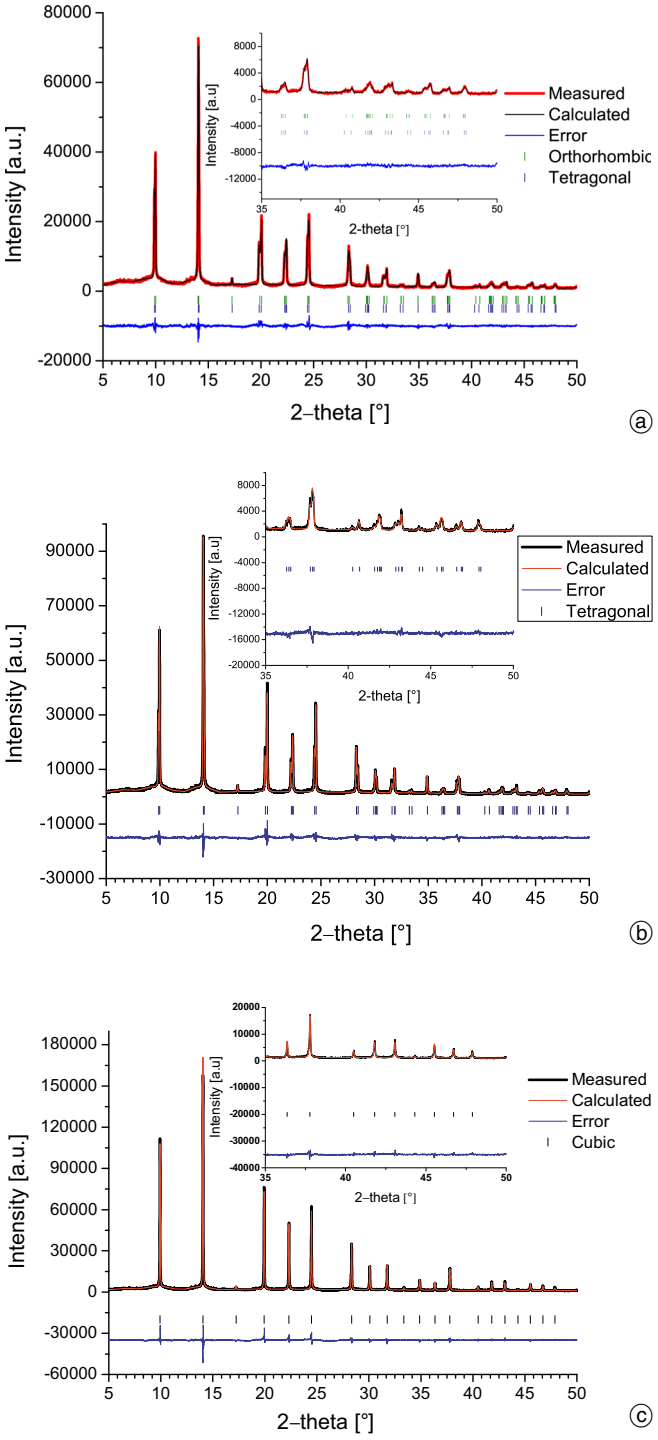

Fig. 1. Measured and calculated synchrotron diffraction profiles and their difference curves for $(K_{0.37}Na_{0.52}Li_{0.03})(Nb_{0.87}Ta_{0.1}Sb_{0.03})O_3$ at (**a**) 20 °C, (**b**) 200 °C and (**c**) 360 °C respectively.

The unit cell parameters as a function of temperature are shown in Fig. 2. The data were refined up to 180 °C using a two-phase analysis approach because the refinement using one phase was not successful. The percentage of the constituent phases present was calculated through the scale factors involving the product of mass and volume of the unit cell contents of each phase. In this tech-

Table 2. Fractional atomic coordinates and isotropic atomic displacement parameters B_{iso} from the synchrotron Rietveld refinement of $(K_{0.37}Na_{0.52}Li_{0.03})(Nb_{0.87}Ta_{0.1}Sb_{0.03})O_3$ ceramics at some selected temperatures (Å^2).

Atom	x	y	z	B_{iso}	Atom	x	Y	z	B_{iso}
Orthorhombic phase (20 °C)					**Tetragonal phase (20 °C)**				
O1	0.5	0.25	0.27(4)	0.0073(11)	O1	0	0.5	0.581(8)	0.0073(11)
O2	0	0	0.565(9)	0.0073(11)	O2	0.5	0.5	0.029(13)	0.0073(11)
Na	0	0	0	0.019(4)	Na	0	0	0	0.015(2)
K	0	0	0	0.019(4)	K	0	0	0	0.015(2)
Li	0	0	0	0.019(4)	Li	0	0	0	0.015(2)
Zr	0	0	0	0.019(4)	Zr	0	0	0	0.015(2)
Nb	0.5	0	0.516(8)	0.0192(12)	Nb	0.5	0.5		0.0105(10)
Ta	0.5	0	0.516(8)	0.0192(12)	Ta	0.5	0.5		0.0105(10)
Sb	0.5	0	0.516(8)	0.0192(12)	Sb	0.5	0.5		0.0105(10)
Orthorhombic phase (100 °C)					**Tetragonal phase (100 °C)**				
O1	0.5	0.25	0.27(5)	0.011(10)	O1	0	0.5	0.562(7)	0.0110(10)
O2	0	0	0.567(11)	0.011(10)	O2	0.5	0.5	0.015(15)	0.0110(10)
Na	0	0	0	0.014(3)	Na	0	0	0	0.0232(10)
K	0	0	0	0.014(3)	K	0	0	0	0.0232(10)
Li	0	0	0	0.014(3)	Li	0	0	0	0.0232(10)
Zr	0	0	0	0.014(3)	Zr	0	0	0	0.0232(10)
Nb	0.5	0	0.520(7)	0.0223(9)	Sb	0.5	0.5	0.505(7)	0.0096(4)
Ta	0.5	0	0.520(7)	0.0223(9)	Nb	0.5	0.5	0.505(7)	0.0096(4)
Sb	0.5	0	0.520(7)	0.0223(9)	Ta	0.5	0.5	0.505(7)	0.0096(4)
Cubic phase (360 °C)					**Tetragonal phase (200 °C)**				
O	0.5	0.5	0	0.0170(7)	O1	0	0.5	0.561(4)	0.0128(10)
Na	0	0	0	0.0274(5)	O2	0.5	0.5	0.003(10)	0.0128(10)
K	0	0	0	0.0274(5)	Na	0	0	0	0.0182(8)
Li	0	0	0	0.0274(5)	K	0	0	0	0.0182(8)
Zr	0	0	0	0.0274(5)	Li	0	0	0	0.0182(8)
Nb	0.5	0.5	0.5	0.02036(20)	Zr	0	0	0	0.0182(8)
Ta	0.5	0.5	0.5	0.02036(20)	Nb	0.5	0.5	0.515(4)	0.0185(2)
Sb	0.5	0.5	0.5	0.02036(20)	Ta	0.5	0.5	0.515(4)	0.0185(2)
					Sb	0.5	0.5	0.515(4)	0.0185(2)

nique, the weight fraction of the phase, (W_P) can be obtained using the following equation;

$$W_p = \frac{S_p(Z,M,V)_p \cdot \tau_j}{\sum_j S_j(Z,M,V)_j \cdot \tau_p}, \quad (1)$$

where W_p is the relative weight fraction of phase p in a mixture of j phases while S, Z, M and V are respectively the Rietveld scale factors derived from the refinement, the number of formula units per unit cell, mass of the formula unit and the unit cell volume.

Table 3. Experimental details and refinement results for $(K_{0.37}Na_{0.52}Li_{0.03})(Nb_{0.87}Ta_{0.1}Sb_{0.03})O_3$ for the lowest temperatures of each model, *i.e.* 20 °C, 200 °C and 360 °C respectively.

Phase type	Two-phase		Single	Single
Crystal system, space group	orthorhombic, *Amm*2	tetragonal, *P*4*mm*	tetragonal, *P*4*mm*	Cubic, *Pm*$\bar{3}$*m*
a (Å)	3.95000(7)	3.95779(6)	3.961364(19)	3.975964(16)
b (Å)	5.6320(2)			
c (Å)	5.6379(3)	3.99799(12)	3.99797(3)	
V (Å^3)	125.422(9)	62.625(2)	62.7378(6)	62.8532(4)
Z	2	1	1	1
Refinement				
R_p (%)	6.5		8.02	7.31
R_{wp} (%)	8.37		6.77	6.7
R_{exp} (%)	3.88		3.6	3.35
GOF	4.2		5.1	5.8
X^2	18.13		26.26	31.97
No of parameters	47	47	47	24

The orthorhombic *Amm*2 (38) and the tetragonal *P*4*mm* (99) space group were chosen for the refinement up to 340 °C while the cubic phase $Pm\bar{3}m$ (221) was used from 360 °C to 400 °C. The first two phases coexisted from 20 °C to 180 °C while only the tetragonal phase was present from 200 °C to 340 °C. For the orthorhombic phase, the cell parameters a_o and c_o increased with increasing temperature while b_o decreased. The orthorhombic cell parameters b_o and c_o were divided by $\sqrt{2}$ for better representation and they fit well with a_t and c_t from the tetragonal phase. The subscript 't' denotes the tetragonal cell. In the tetragonal phase, the c/a-ratio increased up to 80 °C. Above this temperature, a constant decrease of the c/a-ratio could be observed up to the ferroelectric-paraelectric phase transition.

In *Amm*2 space group, the different values of b_o and c_o lead to a rhombic distortion of the $(001)_C$ plane resulting in an expansion along $[110]_C$. The pseudocubic lattice parameter a_{pc} can then be calculated using the formula:

$$a_{pc} = \frac{\sqrt{b_o^2 + c_o^2}}{2} . \qquad (2)$$

The pseudo-monoclinic angle β was derived from the relation;

$$\beta = 2 \arcsin\left(\frac{c_o}{2a_{pc}}\right) . \qquad (3)$$

The plot of the calculated pseudo-monoclinic angle as a function of temperature is shown in Fig. 3. As the values of of b_o and c_o changes (Fig. 2), the pseudo-monoclinic angle increases with temperature.

The sample was polished and later ground to fine powder in preparation for the synchrotron measurement. Quite often this mechanical treatment produces stresses and strains which were introduced to the sample and to release them, the powder was annealed. The diffraction peaks for the patterns at lower temperatures (especially at $T \sim 20$ °C) show that they were significantly broadened.

Microstructural analysis was done with the anisotropic peak broadening model from Stephens [20]. In the tetragonal phase especially, very high strains are reached in the

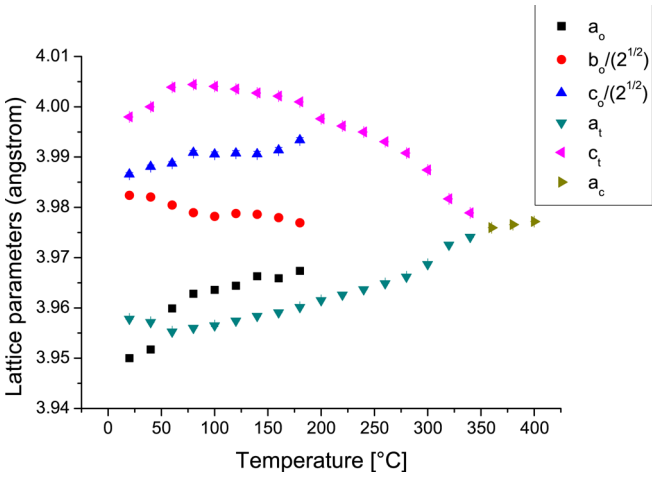

Fig. 2. Temperature dependence of lattice parameters a_o, b_o, c_o for the orthorhombic and a_t, c_t for the tetragonal and a_c for the cubic phase. There is a coexistence of orthorhombic and tetragonal phases between 20 °C and 180 °C, the tetragonal phase solely exists between 180 and 340 °C; the cubic phase exists above 350 °C.

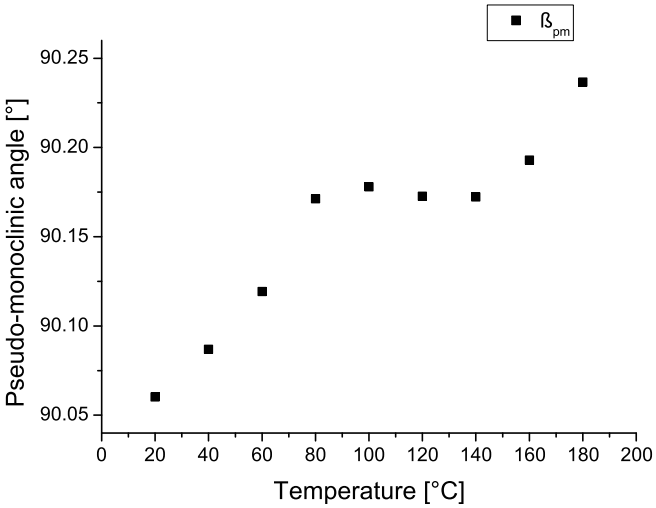

Fig. 3. Pseudo-monoclinic angle as a function of temperature.

polar direction for $00l_t$ reflections. Thus the largest deviations of d-values are found along the polar axes. For lamellar domains, this indicates that the polar axes are oriented along the width of the domains. The best explanation for this configuration is in the 90° domains published for $BaTiO_3$ [22] and PZT [23] instead of 180° domains. A possible explanation for the peak broadening could be that the micro-strains which were introduced during processing were not completely removed by annealing. These anisotropically broadened reflections may result from strain fields which lead to different d-values. At low temperatures, the anisotropic broadening of the peaks can be interpreted in terms of compressive stresses which result in smaller tetragonal c/a ratios. As the temperature is increased, the lattice relaxes, which leads to the formation of larger-sized domains and as a result, a more consistent tetragonal c/a-ratio is obtained.

A plot of the dielectric permittivity as a function of temperature is shown in Fig. 4. The enlarged inset shows the dielectric constant values with a kink at approx. 40 °C. The latter may indicate a first-order phase transition where the

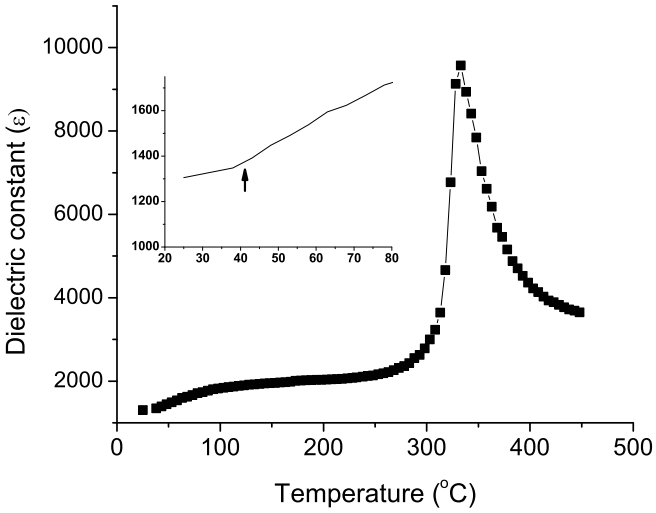

Fig. 4. Variation of the dielectric constant as a function of temperature for $(K_{0.37}Na_{0.52}Li_{0.03})(Nb_{0.87}Ta_{0.1}Sb_{0.03})O_3$ ceramic measured at 1 kHz.

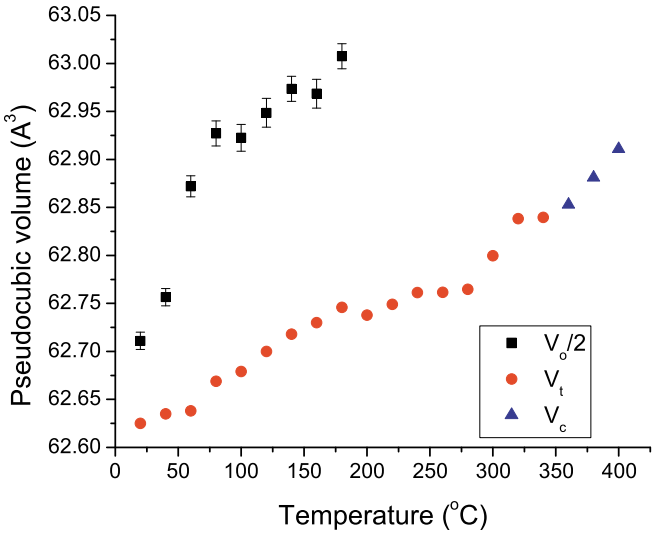

Fig. 5. Unit cell volume for the different phases in $(K_{0.37}Na_{0.52}Li_{0.03})(Nb_{0.87}Ta_{0.1}Sb_{0.03})O_3$ as a function of temperature.

existing phase transforms to another phase but it is difficult to observe in this diagram [7]. The obtained dielectric constant values indicate a maximum at ≈335 °C which corresponds to the temperature of the second order phase transition from tetragonal to the cubic phase. The T_C obtained from the dielectric constant measurement confirms the result of the Rietveld refinement from the X-ray diffraction data.

The unit-cell volume of the orthorhombic, tetragonal and cubic unit cells are shown in Fig. 5. As the temperature increases, the volume of the unit cell also increases but the volume increase for the different phases at low temperatures was not uniform. This behaviour can also be explained by the micro-strains in the sample.

Figure 6 shows the weight fractions of the different phases as a function of temperature. Between 20 and 40 °C, the tetragonal and orthorhombic phases exist at approximately 47 and 53% respectively. Above this temperature, the fraction of the tetragonal phase increases while that of the orthorhombic phase decreases. The reason for this occurrence could be due to relaxation from micro-strain in the sample at near room temperature. The strain

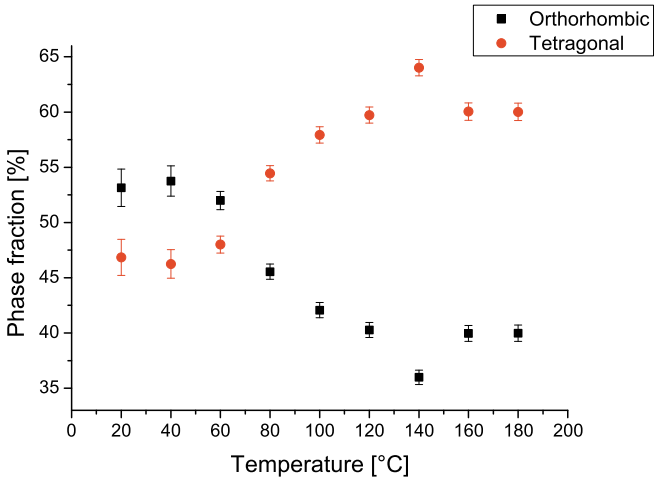

Fig. 6. Weight fractions of the phases in percent as a function of temperature for $(K_{0.37}Na_{0.52}Li_{0.03})(Nb_{0.87}Ta_{0.1}Sb_{0.03})O_3$ calculated according to Eq. (1).

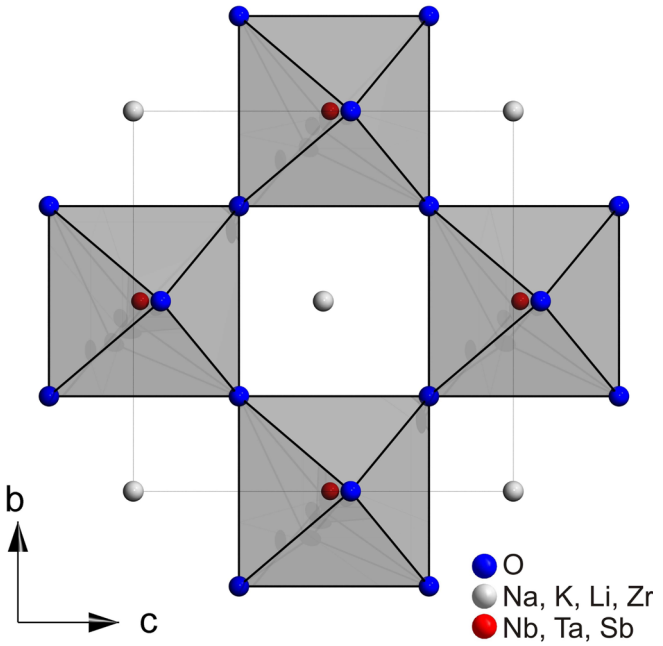

Fig. 7. The polyhedral representation of the structure. The blue spheres represent the oxygen atoms coordinated octahedrally to the red spheres representing Nb, Ta and Sb atoms. The white spheres represent Na, K, Li and Zr at the edges of the unit cell. The image was prepared with the crystallographic software DIAMOND from Crystal Impact.

induces a phase transition to the high temperature phase which maybe accompanied by the formation of domains. Above 180 °C, the weight fraction of the tetragonal phase is 100% while above 340 °C; the weight fraction of the cubic phase is 100%. The theoretical density for this composition at 20 °C was calculated using the mixture rule to be 4.845 g/cm^3. The structure representation of the refined $(K_{0.37}Na_{0.52}Li_{0.03})(Nb_{0.87}Ta_{0.1}Sb_{0.03})O_3$ at 20 °C is shown in Fig. 7. At room temperature the b_o and c_o unit-cell parameters are almost the same, while the a_o unit-cell parameter is shorter (Fig. 2). It should be noted that b_o is along the $[\bar{1}10]_c$-direction and c_o is along the $[110]_c$-direction. When b_o is equivalent to c_o, we have tetragonal symmetry with a polarization vector along $[110]_t$. At low temperatures up to 60 °C a clear two-phase coexistence can be observed with a dominating orthorhombic phase. In this temperature region internal strains from the microstructure decrease with increasing temperature and lead to a relaxation of both phases (Fig. 2 and 3). From 80 °C to 140 °C a continuous phase transition from orthorhombic to tetragonal takes place. Above 140 °C an additional distortion of the orthorhombic phase can be observed (Fig. 3). This unexpected behavior can either be due to strain from tetragonal domain growth or an artifact resulting from the residual anisotropic reflection broadening. This effect is well known for PZT and could be related to real structure effects from the microstructure [24, 25]

Summary

Synchrotron X-ray diffraction measurements have been performed on $(K_{0.37}Na_{0.52}Li_{0.03})(Nb_{0.87}Ta_{0.1}Sb_{0.03})O_3$ cera-

2103805 Kristallographie Heft 2/2011 3B2 Art. zkri1298/Mgbemere w:/p_3/zkri/zkri11_02/1298/zkri.2011.1298.u.3D
gelieferte Daten 11.11.2010 ges.Seiten 7 Bearbeitung in: VMware Universal CS3 Bearb.: Sch.

mics starting from 20 °C to 400 °C using a 20 °C measurement step. Chemical analysis carried out on the sample showed that small amounts of Zr were introduced during the processing and that small amount of some volatile elements (Li, K and Sb) were lost after sintering. The Rietveld refinement method using Fullprof suite has been applied in this work to successfully refine the structure of this ceramic material. An orthorhombic phase with space group *Amm*2, a tetragonal phase with space group *P*4*mm* and a cubic phase with space group $Pm\bar{3}m$ were used to refine the structure from 20 °C to 400 °C. The quantitative analysis showed that while both the orthorhombic and tetragonal phase were present up to 180 °C, only the tetragonal phase remained up to 340 °C and above this temperature, the cubic phase was present.

Acknowledgments. The authors gratefully acknowledge the financial support from Deutsche Forschungsgemeinschaft (DFG) under the grant: SCHN 372/16-1

References

[1] Egerton, L..; Dillion, D. M.: Piezoelectric and dielectric properties of ceramics in the system potassium-sodium niobate. J. Am. Ceram. Soc. **42** (1959) 438-442.

[2] Saito, Y.; Takao, H.; Tani, T.; Nonoyama, T.; Takatori, K.; Homma, T.; Nagaya, T.; Nakamura, M.: Lead-free piezoceramics. Nature. **432** (2004) 84-87.

[3] Noheda, B.; Gonzalo, J. A.; Cross, L. E.; Guo, R.; Park, S. E.; Cox, D. E.; Shirane, G.: Tetragonal-to-monoclinic phase transition in a ferroelectric perovskite: The structure of $PbZr_{0.52}Ti_{0.48}O_3$. Phys. Rev. B. **61** (2000) 8687-8695.

[4] Jaffe, B.; Cook, W. R.; Jaffe, H.: Piezoelectric Ceramics, Academic, New York, 1971, pp. 135.

[5] Zhang, S.; Xia, R.; and Shrout, T. R.: Lead-Free Piezoelectric Ceramics vs. PZT? J. Electroceramics. **19** (2007) 113-126.

[6] Mgbemere, H. E.; Herber, R. -P.; Schneider, G. A.: Effect of MnO_2 on the dielectric and piezoelectric properties of alkaline niobate based lead free piezoelectric ceramics. J. Eur. Ceram. Soc. **29** (2009) 1729-1733.

[7] Akdoðan, E. K.; Kerman, K.; Abazari, M.; Safari, A.: Origin of high piezoelectric activity in ferroelectric $(K_{0.44}Na_{0.52}Li_{0.04})(Nb_{0.84}Ta_{0.1}Sb_{0.06})O_3$ ceramics. Appl. Phys. Lett. **92** (2008) 112908.

[8] Hewat, A. W.: Cubic-tetragonal-orthorhombic-rhombohedral ferroelectric transitions in perovskite potassium niobate: neutron powder profile refinement of the structures. J Phys.C:Solid State Phys. **6** (1973) 2559-2572.

[9] Glazer, A. M.; Megaw, H. D.: Studies of the lattice parameters and domains in the phase transitions of $NaNbO_3$. Acta Cryst. **A29** (1973) 489-495.

[10] Ahtee, M.; Glazer, A. M.: Lattice parameters and tilted octahedra in sodium-potassium niobate solid solutions. Acta Cryst. **A32** (1976) 434-446.

[11] Attia, J.; Bellaiche, L.; Gemeiner, P.; Dkhil, B.; Malic, B.: Study of potassium-sodium-niobate alloys: A combined experimental and theoretical approach. J. Phys. IV France. **128** (2005) 55-60.

[12] Baker, D. W.; Thomas, P. A; Zhang, N.; Glazer, A. M.: Structural study of $K_xNa_{1-x}NbO_3$ (KNN) for compositions in the range x = 0.24–0.36. Acta Cryst. **B65** (2009) 22–28.

[13] Zhang, N.; Glazer, A. M.; Baker, D.; Thomas, P. A.: Structures of $K_{0.05}Na_{0.95}NbO_3$ (50–300 K) and $K_{0.30}Na_{0.70}NbO_3$ (100–200 K). Acta Cryst. **B65** (2009) 291–299.

[14] Knapp, M.; Joco, V.; Baehtz, C.; Brecht, H. H.; Berghaeuser, A.; Ehrenberg, H.; v. Seggern, H.; Fuess, H.: Position-sensitive detector system OBI for high resolution X-ray powder diffraction using on-site readable image plates. Nuclear Instruments and Methods in Physics Research A. **521** (2004) 565-570.

[15] Knapp, M.; Baehtz, C.; Ehrenberg, H.; Fuess, H.: The synchrotron powder diffractometer at beamline B2 at HASYLAB/DESY: status and capabilities. J. Synchrotron Rad. **11** (2004) 328-334.

[16] Rodriguez- Carvajal, J.: Fullprof: A program for Rietveld Refinement and pattern matching analysis. Satellite Meeting on Powder Diffraction of the XV IUCr Congress, **127** (1990).

[17] Laar, B. V.; Yelon, W. B.: The peak in Neutron powder diffraction. J. Appl. Cryst. **17** (1984) 47-54.

[18] Finger, L. W.; Cox, D. E.; Jephcoat, A. P.: A correction for powder diffraction peak assymetry due to axial divergence. J. Appl. Cryst. **27** (1994) 892-900.

[19] Finger, L. W.: PROFVAL: Functions to calculate powder-pattern peak profiles with axial divergence asymmetry. J. Appl. Cryst. **31** (1998) 111.

[20] Stephens, P. W.: Phenomenological model of anisotropic peak broadening in powder diffraction. J Appl. Cryst. **32** (1999) 281-289.

[21] Bergehoff, G.; Berndt, M.; Brandenburg, K.: Evaluation of crystallographic data with the program DIAMOND. J. Res. Natl. Inst. Stand. Technol. **101** (1996) 221–225.

[22] Hu, Y. H.; Chan, H. M.; Wen, Z. X.; and Harmer, M. P.: Scanning Electron Microscopy and Transmission Electron Microscopy Study of Ferroelectric Domains in Doped $BaTiO_3$. J. Am. Ceram. Soc. **69** (1986) 594-602 .

[23] Schmitt, L. A.: Transmissionselektronen mikroskopische Untersuchung der Domänenkonfiguration in $PbZr_{1-x}Ti_xO_3$-Keramiken im Bereich der morphotropen Phasengrenze, Shaker Verlag GmbH, Aachen, (2008).

[24] Schoenau, K. A.; Schmitt, L. A.; Knapp, M.; Fuess, H.; Eichel, R. -A.; Kungl, H.; Hoffmann, M. J.: Nanodomain structure of $Pb[Zr_{1-x}Ti_x]O_3$ at its morphotropic phase boundary: Investigations from local to average structure. Phys. Rev. B **75** (2007) 184117.

[25] Hinterstein, M.; Schoenau, K. A.; Kling, J.; Fuess, H.; Knapp, M.; Kungl, H.; Hoffmann, M. J.: Influence of lanthanum doping on the morphotropic phase boundary of lead zirconate titanate. J. Appl. Phys. **108** (2010) 024110.